Progress In Electromagnetics Research, Vol. 111, 253–269, 2011

ANALYSIS OF A CIRCULAR WAVEGUIDE LOADED WITH DIELECTRIC AND METAL DISCS

V. Kesari

Microwave Tube Research and Development Centre
Bangalore, India

J. P. Keshari

Galgotias College of Engineering and Technology
Greater Noida, India

Abstract—A circular waveguide loaded with dielectric and metal discs was chosen to evaluate its dispersion characteristics and dispersion shaping with change of structure parameters for wideband coalescence of beam- and waveguide-mode dispersion characteristics for wideband gyro-TWT performance. The azimuthally symmetric TE-mode analysis of the structure was carried out in field matching technique by considering the propagating wave in cylindrical free-space region having radius equal to the hole-radius of metal disc, and the stationary waves in free-space and dielectric regions between two consecutive metal discs. The dispersion relation and, in accordance, a computer code were developed. Further, the roots of the dispersion relation for various sets of the structure parameters were obtained using the developed computer code; the dispersion characteristics were plotted; and the dispersion shaping was projected for typically chosen TE_{01}-, TE_{02}- and TE_{03}-modes. The analytical results were validated against those obtained for the conventional and earlier published structures, and also those obtained using commercially available simulation tool. Finally, a study on azimuthal electric field available over the radial coordinate was carried out to show the control of structure parameter on the gyrating electron beam position for the chosen operating mode of a dielectric and metal discs loaded gyro-TWT.

Received 2 November 2010, Accepted 2 December 2010, Scheduled 9 December 2010
Corresponding author: Jaishanker Prasad Keshari (jaishanker_keshari@yahoo.co.in).

1. INTRODUCTION

In photonics and microwave community, the applicability of the periodic structures, such as, in cylindrical optical fibers with helical windings [1], photonic band gap structures for solid-state lasers [2–5], electromagnetic filters [6–10], phase shifters [9–11], polarizers [10, 11], antennas [3, 9–12], antenna feeds [6, 11–13], linear/particle accelerators [14, 15], backward-wave oscillators (BWOs) [9, 16], magnetrons [17], travelling-wave tube (TWT) amplifiers [18–22], cyclotron masers [23, 24], gyrotron sources [25–27] and amplifiers [27–42], etc., exert a pull on their analytical study.

During the last three decades, the axial or the azimuthal periodic structures have shown the applicability in gyro-devices as beam-wave interaction structures [23–40, 42]. The azimuthal periodicity, which has been used in interaction-cavity for mode rarefaction in gyrotron [25–27], predicts a broadbanding in conventional helix-TWT [20], whereas a higher interaction impedance and in turn higher gain performance of gyro-travelling wave tubes (gyro-TWTs), if considered in interaction structure [28, 29]. On the other hand, the axial periodicity in the interaction structure promises higher gain performance in conventional helix-TWT [20] and a wider bandwidth through dispersion shaping of the gyro-TWT [30–40]. In the past, the non-periodic continuous dielectric, in the form of wall-lining or coaxial rod, in circular waveguide was proposed for dispersion shaping to wideband coalescence between the beam- and waveguide-mode dispersion characteristics that in turn signifies the broadband gain-frequency response of a gyro-TWT [41]. While the dielectric loading promises a broadband performance and the attenuator effects for self and parasitic oscillations, it brings the problem of dielectric charging and associated heating in case of lossy dielectrics. Therefore, all metal structures attracts the notice of gyro-TWT developers to play a role of interaction structure, wherein the corrugations control the shape of waveguide-mode dispersion characteristics for broadband device performance.

Choe and Uhm [37] analyzed the infinitesimally thin disc-loaded circular waveguide considering the lowest order stationary- and propagating-wave modes in the disc-occupied and disc-free regions, respectively, while using field matching technique, and showed the control of the waveguide-mode dispersion characteristics by changing the structure parameters. Kesari et al. [30–34] improved the analysis taking higher order stationary- and propagating-wave modes, and first ignoring [31] and then considering [32] finite disc thickness. Combining the advantages of metal and dielectric loading, Kesari et al. [34]

suggested a circular waveguide alternatively loaded with metal and dielectric discs [34]. Similar structure was also analyzed in [16] for it dispersion characteristics with and without presence of annular electron beam, and the instability performance was studied [16].

Taking a turn towards coaxial waveguide, Keasri [35, 36] proposed the coaxial-disc-loaded circular waveguide in two configurations: (i) metal discs are radially projecting inward from the metallic envelope, and (ii) metal discs are radially projecting outward from the coaxial insert, and concluded that the configuration (ii) would be more promising interaction structure. In his work, he has, not only, analyzed the beam-absent case [35] but also the beam-present case [36] for both the configurations. Yue et al. [39] has also analyzed a coaxial circular waveguide using field matching technique, however, the grooves were appearing on the wall of the waveguide, only, and the shape of the groove was chosen arbitrary, which was profiled by a series of rectangular steps [39].

In the past work [34], the authors have considered the hole-radii of metal and dielectric discs same, however, for the present study, alternate dielectric and metal disc-loading has been considered, such that the inner radius of metal discs is less than that of dielectric discs (Fig. 1). The present study has been chosen to monitor the effect of change of amount of dielectric, keeping the metal loading same. The authors restrict themselves to the beam-absent analysis to explore the effect of all the structure parameters on the dispersion characteristics. The analysis (Section 2) starts with writing the field intensity components for three different regions of the structure, which may be substituted to the EM boundary conditions, and the field constants are eliminated to obtain the dispersion relation of the structure. A computer code is developed to find the roots of the dispersion relation for plotting the dispersion characteristics and the

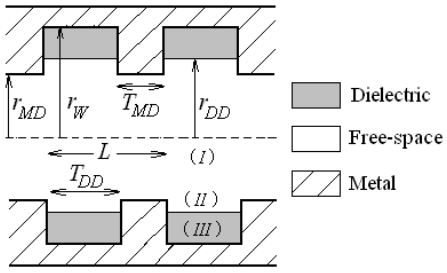

Figure 1. Cut-view of circular cylindrical metal waveguide alternatively loaded with dielectric and metal annular discs.

effects of structures parameters are studied (Section 3). Finally, the study is concluded (Section 4).

2. ANALYSIS FOR BEAM-ABSENT DISPERSION RELATION

Consider a circular waveguide consisting of alternate dielectric and metal discs, such that the inner radius of metal discs is less than that of dielectric discs. For the purpose of analysis, one may divide the structure into three regions. In the cross-section view, one may define the regions as: i) region I: $0 \leq r < r_{MD}$; ii) region II: $r_{MD} \leq r < r_{DD}$; and iii) region III: $r_{DD} \leq r < r_W$, where r_{MD} and r_{DD} are the inner radii of metal and dielectric discs, respectively. r_W is the waveguide radius. One may consider the thicknesses of the metal and dielectric discs as T_{MD} and T_{DD}, respectively, that makes the axial periodicity of the structure, as $L = T_{MD} + T_{DD}$. It is being considered that the region I (disc free region) supports propagating, and regions II and III (disc occupied regions) support standing waves. The axial magnetic and azimuthal electric field intensities are, respectively, as [30–37]:

In region I:

$$H_z^I = \sum_{n=-\infty}^{+\infty} A_n^I J_0\{\gamma_n^I r\} \exp j(\omega t - \beta_n z) \tag{1}$$

$$E_\theta^I = j\omega\mu_0 \sum_{n=-\infty}^{+\infty} \frac{1}{\gamma_n^I} A_n^I J_0'\{\gamma_n^I r\} \exp j(\omega t - \beta_n z) \tag{2}$$

In region II:

$$H_z^{II} = \sum_{m=1}^{\infty} [A_m^{II} J_0\{\gamma_m^{II} r\} + B_m^{II} Y_0\{\gamma_m^{II} r\}] \exp(j\omega t) \sin(\beta_m z) \tag{3}$$

$$E_\theta^{II} = j\omega\mu_0 \sum_{m=1}^{\infty} \frac{1}{\gamma_m^{II}} [A_m^{II} J_0'\{\gamma_m^{II} r\} + B_m^{II} Y_0'\{\gamma_m^{II} r\}] \exp(j\omega t) \sin(\beta_m z) \tag{4}$$

In region III:

$$H_z^{III} = \sum_{m=1}^{\infty} A_m^{III} Z_0\{\gamma_m^{III} r\} \exp(j\omega t) \sin(\beta_m z) \tag{5}$$

$$E_\theta^{III} = j\omega\mu_0 \sum_{m=1}^{\infty} \frac{1}{\gamma_m^{III}} A_m^{III} Z_0'\{\gamma_m^{III} r\} \exp(j\omega t) \sin(\beta_m z) \tag{6}$$

where $Z_0\{\gamma_m^{III} r\} = J_0\{\gamma_m^{III} r\} Y_0'\{\gamma_m^{III} r_W\} - J_0'\{\gamma_m^{III} r_W\} Y_0\{\gamma_m^{III} r\}$; J_0 and Y_0 are the *zero*th order Bessel functions of the first and second kinds, respectively. Prime with a function represents the derivative with respect to its argument. A_n^I, A_m^{II}, B_m^{II} and A_m^{III} are the field constants in different analytical regions, identified by given superscript, respectively. $\gamma_n^I [= (k^2 - \beta_n^2)^{1/2}]$, $\gamma_m^{II} [= (k^2 - \beta_m^2)^{1/2}]$, and $\gamma_m^{III} [= (\varepsilon_r k^2 - \beta_m^2)^{1/2}]$ are the radial propagation constants in regions I, II, and III, respectively. $\beta_n [= \beta_0 + 2\pi\, n/L]$ is the axial phase propagation constant in disc free region I; here, β_0 is the axial phase propagation constant for fundamental space harmonic, and $n[= 0, \pm 1, \pm 2, \pm 3, \ldots]$ is space harmonic number. β_m $[= m\pi/T_{DD}]$ is the axial propagation constant in disc occupied regions (II and III); here, $m[= 1, 2, 3, \ldots]$ is the modal harmonic number.

In order to characterise the structure, one may write the relevant boundary conditions, stating the continuity of the tangential components of electric and magnetic field intensities at the interface, $r = r_{MD}$, between the free-space disc-free region (I) and disc-occupied free-space region (II) (Fig. 1) as well as the vanishing tangential component of electric field intensity at the metal inner circumferential edge of the discs, $r = r_{MD}$, those may be written as

$$E_\theta^I = \begin{cases} E_\theta^{II} & 0 < z < T_{DD} \\ 0 & T_{DD} \le z \le L \end{cases} \quad (r = r_{MD}) \tag{7}$$

$$H_z^I = H_z^{II} \qquad 0 < z < T_{DD} \quad (r = r_{MD}); \tag{8}$$

and at the interface, $r = r_{DD}$, between the free-space (II) and dielectric-filled (III) disc-occupied regions (Fig. 1) may be put as:

$$E_\theta^{II} = E_\theta^{III} \qquad 0 < z < T_{DD} \quad (r = r_{DD}) \tag{9}$$

$$H_z^{II} = H_z^{III} \qquad 0 < z < T_{DD} \quad (r = r_{DD}). \tag{10}$$

One may substitute the field expressions from (3)–(6) into (9) and (10) to represent B_m^{II} in terms of A_m^{II} while eliminating A_m^{III} from the resulting relations, as:

$$\frac{B_m^{II}}{A_m^{II}} = \frac{\begin{matrix} \gamma_m^{III} J_0'\{\gamma_m^{II} r_{DD}\} Z_0\{\gamma_m^{III} r_{DD}\} \\ -\gamma_m^{II} J_0\{\gamma_m^{II} r_{DD}\} Z_0'\{\gamma_m^{III} r_{DD}\} \end{matrix}}{\begin{matrix} \gamma_m^{II} Y_0\{\gamma_m^{II} r_{DD}\} Z_0'\{\gamma_m^{III} r_{DD}\} \\ -\gamma_m^{III} Y_0'\{\gamma_m^{II} r_{DD}\} Z_0\{\gamma_m^{III} r_{DD}\} \end{matrix}} = \xi(say). \tag{11}$$

Now, one may express the field constants A_m^{II} $(m = 1, 2, 3, \ldots)$, in terms of a series involving A_n^I $(-\infty < n < \infty)$. For this purpose, one may substitute the field expressions (1) and (3), where in later B_m^{II} is represented in terms of A_m^{II} using (11), into the boundary condition (8),

multiply it by $\sin(\beta_m z)$, then integrate it between $z = 0$ and $z = T_{DD}$, to obtain:

$$A_m^{II} = \sum_{n=-\infty}^{\infty} A_n^I \, U_{n\,m} \tag{12}$$

where

$$U_{nm} = \frac{2}{T_{DD}} \frac{J_0\{\gamma_n^I r_{MD}\}}{[J_0\{\gamma_m^{II} r_{MD}\} + \xi Y_0\{\gamma_m^{II} r_{MD}\}]} \frac{\beta_m[1-(-1)^m \exp(-j\beta_n T_{DD})]}{(\beta_m^2 - \beta_n^2)}.$$

Similarly, one may obtain another series expression, similar to (12), for A_m^{II}, but now with the help of the field expressions (2) and (4), instead of (1) and (3), respectively, and the boundary condition (7), instead of (8), and by changing the integration limits to $z = 0$ and $z = L$, instead of $z = 0$ and $z = T_{DD}$, as follows:

$$A_m^{II} = \sum_{n=-\infty}^{\infty} A_n^I \, S_{n\,m} \tag{13}$$

where

$$S_{nm} = \frac{2\gamma_m^{II} J_0'\{\gamma_n^I r_{MD}\}[\beta_m - \exp(-j\beta_0 L)[\beta_m \cos(\beta_m L) + j\beta_n \sin(\beta_m L)]]}{\gamma_n^I [J_0'\{\gamma_m^{II} r_{MD}\} + \xi Y_0'\{\gamma_m^{II} r_{MD}\}](\beta_m^2 - \beta_n^2) T_{DD}}.$$

Then, the following relation results by equating the right hand sides of (12) and (13):

$$\sum_{n=-\infty}^{\infty} A_n^I \, (U_{nm} - S_{nm}) = 0. \tag{14}$$

Choosing to take the same number υ, say, of the values of the stationary-wave modal number (m) as that of space harmonic number (n) (typically, $\upsilon = 7$, $n = 0, \pm 1, \pm 2, \pm 3$, and $m = 1, 2, 3, 4, 5, 6, 7$), one can form υ number of simultaneous equations in the field constants A_n^I (typically, seven equations in $A_0^I, A_{\pm 1}^I, A_{\pm 2}^I, A_{\pm 3}^I$) with the help of (14). The condition for the non-trivial solution, that the determinant formed by the coefficients of the filed constants occurring in these equations is zero, yields the following dispersion relation of the circular waveguide loaded with dielectric and metal discs:

$$\begin{aligned} &\det \big| M_{n\,m} \, J_0\{\gamma_n^I r_{MD}\} \; [J_0'\{\gamma_m^{II} r_{MD}\} + \xi \, Y_0'\{\gamma_m^{II} r_{MD}\}] \\ - \; &J_0'\{\gamma_n^I r_{MD}\}[J_0\{\gamma_m^{II} r_{MD}\} + \xi \, Y_0\{\gamma_m^{II} r_{MD}\}] \big| = 0 \\ &\qquad\qquad (-\infty < n < \infty, 1 \le m < \infty) \end{aligned} \tag{15}$$

where

$$M_{nm} = \frac{\gamma_n^I \beta_m [1 - (-1)^m \exp(-j\beta_n T_{DD})]}{\gamma_m^{II} \, [\beta_m - \exp(-j\beta_0 L)[\beta_m \cos(\beta_m L) + j\beta_n \sin(\beta_m L)]]}. \tag{16}$$

3. RESULTS AND DISCUSSION

In order to validate the dispersion relation (15) through (16) with reference to the special cases of the structure, one may consider $r_{DD} = r_{MD}$, which passes (15) as that published for alternate dielectric and metal discs loaded circular waveguide [34]. Further, one may consider either $r_{DD} = r_W$ or $\varepsilon_r = 1$, in both the cases the radial propagation constant in region II becomes same as that in region III ($\gamma_m^{II} = \gamma_m^{III}$), which in turn gives a relation $J_0\{\gamma_m^{II} r_{MD}\} + \xi\, Y_0\{\gamma_m^{II} r_{MD}\} = Z_0\{\gamma_m^{II} r_{MD}\}$ that passes (15) as that published for all metal disc-loaded circular waveguide [32] (Fig. 2). For the special case of $T_{DD} = L$ and $\varepsilon_r = 1$, (15) passes to that published for infinitesimally thin disc-loaded circular waveguide [31], which further for the case of ignoring the harmonics passes to that published by Choe and Uhm [37]. For the very basic special case, considering either $r_{MD} = r_{DD} = r_W$ or $r_{MD} = r_W$ with $\varepsilon_r = 1$, the dispersion relation passes to that for smooth-wall circular waveguide.

The dispersion characteristics of the structure for the various combinations of structure parameters may be obtained by solving the dispersion relation (15) through (16). For the purpose, a computer code is developed in MATLAB in accordance with (15). In general, due to the axial periodicity of the structure, it shows a periodic dispersion characteristics such that it shows points of zero group velocity at $\beta_0 L = v\pi$, where $v = 0, 1, 2, \ldots$ showing alternate stop- and pass-bands (Figs. 2–7). Here, it is necessary to validate the analytical results obtained using the present analysis with those obtained using

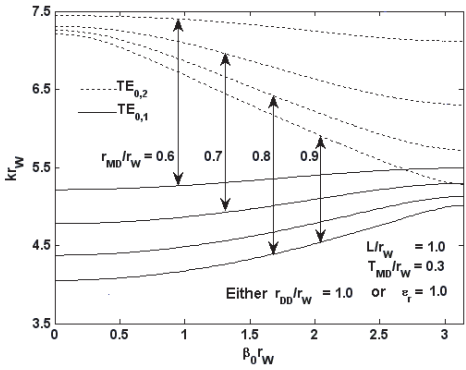

Figure 2. Validation of dispersion characteristics of the considered structure against that of all metal disc-loaded circular waveguide [32] for the modes TE_{01} (solid curve) and TE_{02} (broken curve).

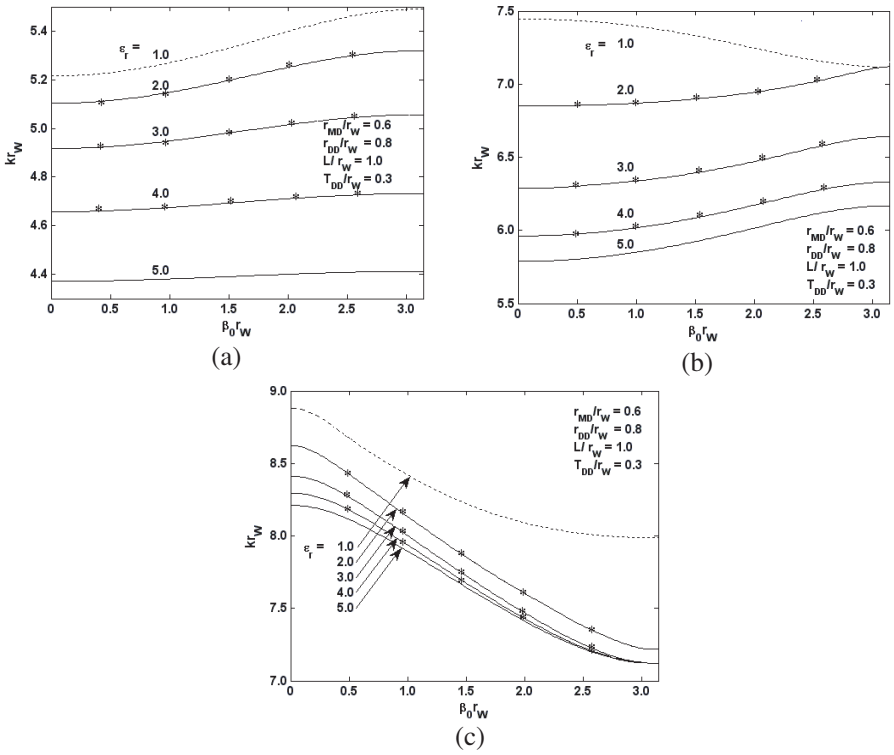

Figure 3. Dispersion characteristics of the considered structure for the modes (a) TE_{01}, (b) TE_{02}, and (c) TE_{03}, taking relative permittivity of dielectric disc as the parameter. (Broken curve: all metal structure; Star markers: HFSS results).

commercially available simulation software, such as HFSS. For the purpose, the model of the structure is created in HFSS workspace and the analysis is carried out. It is fascinating to note that the results obtained by two independent methods, for typically chosen modes and the structures parameters, are within 3% (Fig. 3). For both the TE_{01} and TE_{02} modes, with the increase of the relative permittivity of the dielectric discs, the lower and upper cutoff frequencies shift to lower value. Quantitatively, for the TE_{01} mode, the shift in upper cutoff frequency is higher than that of lower cutoff frequency, which in turn shortens the passband (Fig. 3(a)); whereas, for the TE_{02} mode, the shift in lower and upper cutoff frequencies are almost equal, effectively the passband does not change (Fig. 3(b)). It is interesting to note that in absence of the dielectric discs, the group velocity takes zero value follows by negative values to reach again zero and further positive over

the propagation constant axis, whereas, in presence of the dielectric discs, it takes zero value follows by positive values to reach again zero and further negative (Fig. 3(b)), i.e., the inclusion of dielectric turns the negative dispersion into positive. For the TE_{03} mode, for the both cases of absence and presence of the dielectric discs, the group velocity takes zero value follows by negative values to reach again zero and further positive, however, with the increase of the relative permittivity of the dielectric discs, quantitatively the shift of lower cutoff frequency is higher than that of upper cutoff frequency, which in turn widens the passband. It has been observed that in presence of dielectric discs upper cutoff frequency shifts to lower value, whereas the lower cutoff frequency remains unchanged with the increase of the relative permittivity of the dielectric discs and shortens the passband (Fig. 3(c)).

For the TE_{01} mode, with the increase of dielectric disc radius, for constant metal disc radius, the lower and upper cutoff frequencies shifts up, however, quantitatively the shift in lower cutoff frequency is less than that of upper cutoff frequency, which increases the passband (Fig. 4(a)). Similarly, for the TE_{02} mode, the passband increases with the increase of dielectric disc radius. Here, it has been observed that the shift in frequency is very specifically defined for the dielectric disc radius, for example, for the taken structure parameters ($r_{MD}/r_W = 0.6$, $L/r_W = 1.0$, $T_{DD}/r_W = 0.3$, and $\varepsilon_r = 5.0$) the frequency shift is maximum for r_{DD}/r_W equal to 0.8 to 0.9, and minimum for 0.7 to 0.8, where as for r_{DD}/r_W equal to 0.6 to 0.7 is found in between (Fig. 4(b)). For the TE_{03} mode, for the lower values of inner dielectric disc radius, the group velocity takes zero value follows by positive values to reach again zero and further negative, whereas for higher values of inner dielectric disc radius, it takes zero value follows by negative values to reach again zero and further positive over the propagation constant axis. Interestingly, in the process of changing the inner dielectric disc radius, the frequency corresponding to the point of $\beta_0 L = v\pi$, where $v = 1, 3, 5, \ldots$, remains almost unchanged (Fig. 4(c)). The change of group velocity close to $\beta_0 = 0$ (operating point of a gyro-TWT) due to r_{DD}/r_W may be utilized to avoid the negative group velocity close to $\beta_0 = 0$, that may be the reason for oscillation in the device.

In general, with the increase of periodicity of the structure, both the lower and upper cutoff frequencies shift down and shorten the passband with higher relative shift in upper cutoff frequency than that of lower. Clearly, the reflection of the change of the periodicity of the structure may be observed as the change in period of the dispersion characteristics, for all the three modes considered. For the TE_{01} and TE_{02} modes, the group velocity takes zero value follows by positive

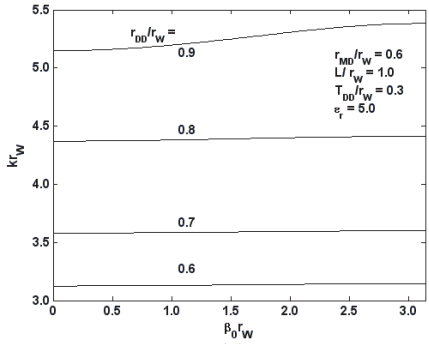

(a)

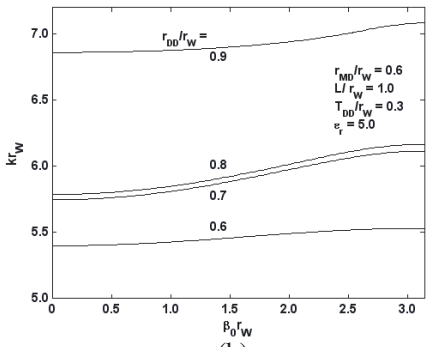

(b)

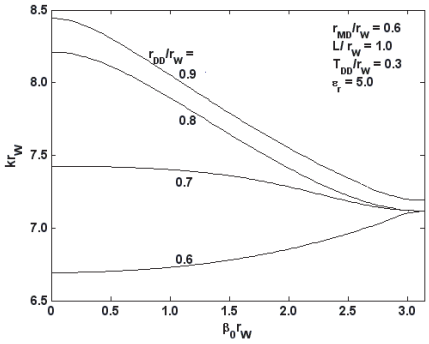

(c)

Figure 4. Dispersion characteristics of the considered structure for the modes (a) TE_{01}, (b) TE_{02}, and (c) TE_{03}, taking inner radius of dielectric disc as the parameter.

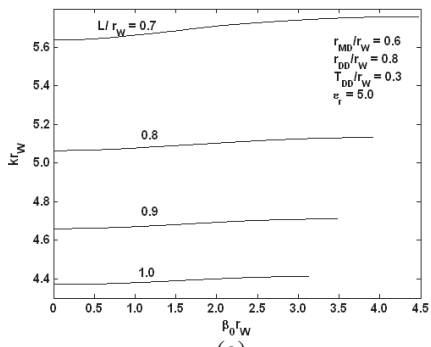

(a)

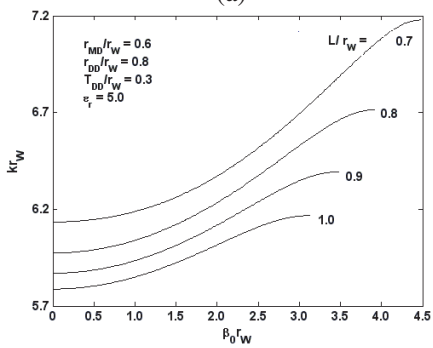

(b)

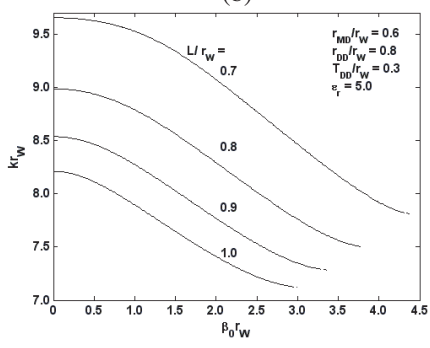

(c)

Figure 5. Dispersion characteristics of the considered structure for the modes (a) TE_{01}, (b) TE_{02}, and (c) TE_{03}, taking periodicity as the parameter.

values to reach again zero and further negative, whereas for the TE_{03} mode, it takes zero value follows by negative values to reach again zero and further positive over the propagation constant axis (Fig. 5). Similar to the all metal disc-loaded waveguide without dielectric discs, the shape of the dispersion characteristics and the passband is not very sensitive to the change of dielectric disc thickness, however, with the decrease of the dielectric disc thickness or with the increase of metal disc thickness, the passband shifts to lower frequency side for the TE_{01} and TE_{02} modes (Figs. 6(a) and 6(b)). For the TE_{03} mode, the shape of the dispersion characteristics and the passband is least sensitive to the change of dielectric disc thickness, if very precisely seen, the lower cutoff frequency is insensitive and the upper cutoff frequency first decreases and then increases with decrease of dielectric disc thickness or with increase of metal disc thickness (Fig. 6(c)).

Further, for the constant difference between the radii of metal and dielectric discs, the lower and upper cutoff frequencies shift to higher value and passband increases with increase of metal disc radius for the TE_{01} and TE_{02} modes (Figs. 7(a) and 7(b)), where as a major change of dispersion characteristics and the passband has been observed for the TE_{03} mode (Fig. 7(c)). It should also be noted here that for the TE_{03} mode the dispersion characteristics is very specific for each set of structure parameters considered (Fig. 7(c)).

In order to estimate, qualitatively, the available azimuthal electric field for interaction with gyrating electron beam, one may plot the azimuthal electric field intensity (E_θ^I) distribution over the radial coordinate of considered structure within the free-space region inside the metal-disc-hole for the operating mode. For the purpose, one has to substitute roots of the dispersion relation (15) into the field intensity component (2). For simplicity, $J_0'\{\gamma_n^I r\}$, which is directly proportional to E_θ^I, is plotted against normalized radial coordinate r/r_W close to the waveguide cut-off frequency at $\beta_0 = 0$ where the gyro-TWT is operated to reduce the effect of velocity spread and pulse distortion. The gyrating electron beam will be positioned at the maxima of E_θ^I in free-space region of the considered structure, taking this into account, distribution of azimuthal electric field intensity has been considered over the horizontal axis running up to $r/r_W = r_{MD}/r_W$ (Fig. 8). For a particular mode considered, with the decrease of r_{DD}/r_W, the possible beam position shifts away from guide axis. On the other hand, in order to study the effect of change of the modes for constant r_{DD}/r_W, the possible beam position shifts closer to guide axis with increasing azimuthal mode number of the operating mode (Fig. 8). Here, it is interesting to note that the structure provides a control over the position of the gyrating electron beam.

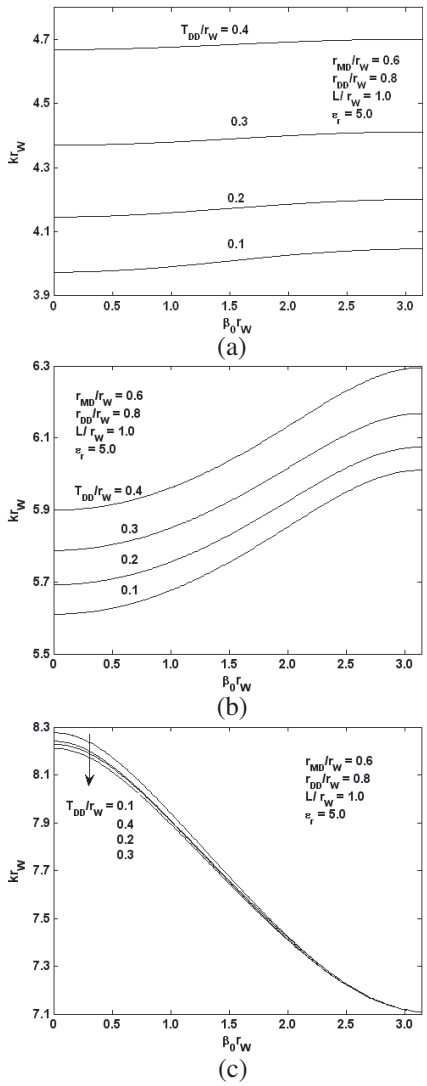

Figure 6. Dispersion characteristics of the considered structure for the modes (a) TE_{01}, (b) TE_{02}, and (c) TE_{03}, taking thickness of dielectric disc as the parameter.

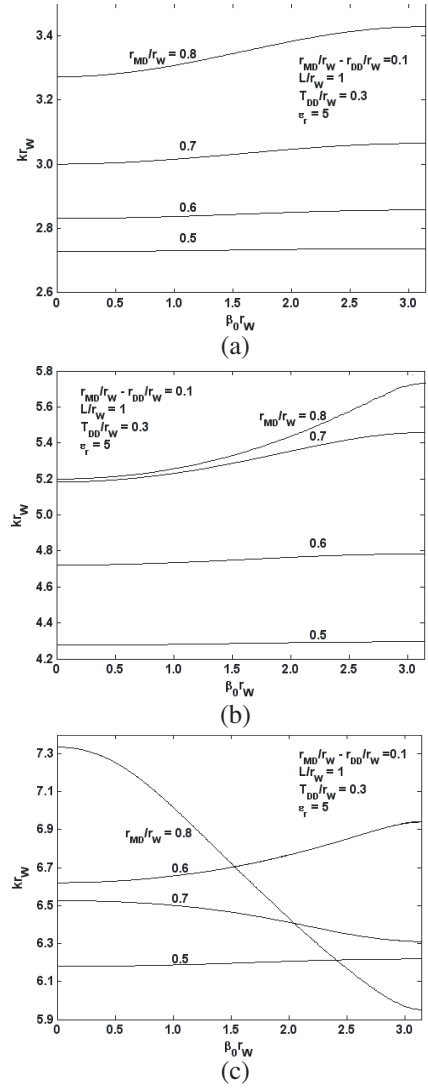

Figure 7. Dispersion characteristics of the considered structure for the modes (a) TE_{01}, (b) TE_{02}, and (c) TE_{03}, taking radius of metal disc as the parameter such that $r_{MD}/r_W - r_{DD}/r_W = 0.1$.

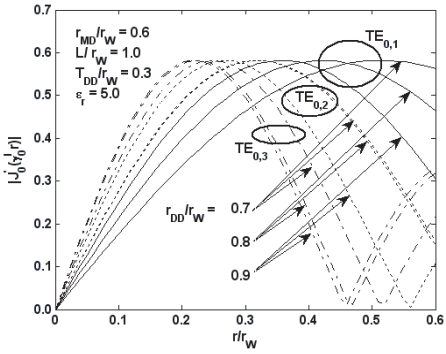

Figure 8. Azimuthal electric field intensity distribution over the radial coordinate (r/r_W) of the considered structure for the TE_{01}, TE_{02}, and TE_{03} modes taking inner radius of dielectric disc as the parameter.

4. CONCLUSION

The dispersion characteristics of the alternately dielectric and metal discs loaded circular waveguide has shown a control over the shape and the passband, as well as over the position of the gyrating electron beam (in case of a gyro-TWT), with the change of structure parameters for the typically chosen three modes. For the sake of present study, the dispersion characteristics of the considered structure and the effect of structure parameters on its shape have been evaluated for the purpose of getting a straight line portion of the dispersion characteristics over a wideband frequency range, which in turn tells the wideband gyro-TWT performance. The authors are aware that the study of dispersion shaping can only qualitatively predicts the possibility of broadbanding a gyro-TWT. For getting a realistic picture of broadbanding, as was earlier done for metal vane-loaded [28] or annular metal disc-loaded [30, 32] or coaxial-disc-loaded [36] or dielectric-loaded [41] or helix-loaded [42] gyro-TWTs, one has to substitute the propagation constant predicted by the cold/beam-absent analysis of the loaded structure into the beam-present dispersion relation of a gyro-TWT, which will be subsequently interpreted for the small-signal device gain. However, the related study is kept out of the perimeter of the present study.

REFERENCES

1. Kumar, D., P. K. Choudhury, and O. N. Singh II, "Towards the dispersion relations for dielectric optical fibers with helical

windings under slow- and fast-wave considerations — A comparative analysis," *Progress In Electromagnetics Research*, Vol. 80, 409–420, 2008.

2. Wu, C.-J., Y.-H. Chung, B.-J. Syu, and T.-J. Yang, "Band gap extension in a one-dimensional ternary metal-dielectric photonic crystal," *Progress In Electromagnetics Research*, Vol. 102, 81–93, 2010.
3. Lin, H.-N. and C.-C. Tang, "Analysis and design for high-gain antenna with periodic structures," *PIERS Online*, Vol. 6, No. 2, 181–184, 2010.
4. Xie, H.-H., Y.-C. Jiao, K. Song, and Z. Zhang, "A novel multi-band electromagnetic band-gap structure," *Progress In Electromagnetics Research Letters*, Vol. 9, 67–74, 2009.
5. Escorcia-García, J. and M. E. M. Mora-Ramos, "Study of optical propagation in hybrid periodic/quasiregular structures based on porous silicon," *PIERS Online*, Vol. 5, No. 2, 167–170, 2009.
6. Dai, G. and M. Xia, "Novel miniaturized bandpass filters using spiral-shaped resonators and window feed structures," *Progress In Electromagnetics Research*, Vol. 100, 235–243, 2010.
7. Yang, M., J. Xu, Q. Zhao, L. Peng, and G. Li, "Compact, broad-stopband lowpass filters using sirs-loaded circular hairpin resonators," *Progress In Electromagnetics Research*, Vol. 102, 95–106, 2010.
8. Chiou, Y.-C., P.-S. Yang, J.-T. Kuo, and C.-Y. Wu, "Transmission zero design graph for dual-mode dual-band filter with periodic stepped-impedance ring resonator," *Progress In Electromagnetics Research*, Vol. 108, 23–36, 2010.
9. Amari, S., R. Vahldieck, J. Bornemann, and P. Leuchtmann, "Spectrum of corrugated and periodically loaded waveguides from classical matrix eigenvalues," *IEEE Trans. Microwave Theory Tech.*, Vol. 48, 453–460, 2000.
10. Amari, S., R. Vahldieck, and J. Bornemann, "Analysis of propagation in periodically loaded circular waveguide," *IEE Proc. Microwave Antennas Propagation*, Vol. 146, No. 1, 50–54, 1999.
11. Clarricoats, P. J. B. and A. D. Olver, *Corrugated Horns for Microwave Antennas*, Peter Peregrinus, London, 1984.
12. Heydari, R. D., H. R. Hassani, and A. R. Mallahzadeh, "A new 2–18 GHz quad-ridged horn antenna," *Progress In Electromagnetics Research*, Vol. 81, 183–195, 2008.
13. Uher, J., J. Bornemann, and U. Rosenberg, *Waveguides Components for Antenna Feed Systems: Theory and CAD*, Artech

House, Norwood, 1993.

14. Shi, W., L. Yuzheng, and T. Higo, "A new method for dispersion curves of HOM in periodical axisymmetric accelerating structures," *Proc. 2nd Asian Particle Accelerator Conf.*, 153–155, Beijing, China, 2001.
15. Hu, Y., C. Tang, H. Chen, Y. Lin, and D. Tong, "An X-band disk and washer accelerating structure for electron accelerators," *Proc. Particle Accelerator Conf.*, 975–977, Chicago, 2001.
16. Amin, M. R. and K. Ogura, "Dispersion characteristics of a rectangularly corrugated cylindrical slow-wave structure driven by a non-relativistic annular electron beam," *IET Microwave Antennas Propag.*, Vol. 1, No. 3, 575–579, 2007.
17. Ding, S., B. Jia, F. Li, and Z. Zhu, "3D simulation of 18-vane 5.8 GHz magnetron," *Journal of Electromagnetic Waves and Applications*, Vol. 22, No. 14–15, 1925–1930, 2008.
18. Malek, F., "The analytical design of a folded waveguide traveling wave tube and small signal gain analysis using Madey's theorem," *Progress In Electromagnetics Research*, Vol. 98, 137–162, 2009.
19. Mulcahy, T., H. Song, and F. Francisco, "New method of integrating periodic permanent magnet (PPM) assembly in traveling wave tubes (TWTs)," *Progress In Electromagnetics Research C*, Vol. 10, 187–199, 2009.
20. Jain, P. K. and B. N. Basu, "Electromagnetic wave propagation through helical structures," *Electromagnetic Fields in Unconventional Materials*, O. N. Singh and A. Lakhtakia, Ed., John Wiley & Sons, USA, 2000.
21. Zhu, Z. J., B. F. Jia, and D. M. Wan, "Efficiency improvement of helix traveling-wave tube," *Journal of Electromagnetic Waves and Applications*, Vol. 22, No. 13, 1747–1756, 2008.
22. Duan, Z. Y., Y. B. Gong, Y. Y. Wei, W. X. Wang, B.-I. Wu, and J. A. Kong, "Efficiency improvement of broadband helix traveling wave tubes using hybrid phase velocity tapering model," *Journal of Electromagnetic Waves and Applications*, Vol. 22, No. 7, 1013–1023, 2008.
23. Jerby, E. and G. Bekefi, "Cyclotron maser experiments in a periodic wave guide," *Phys. Rev. E*, Vol. 48, No. 6, 4637–4641, 1993.
24. Chu, K. R., "The electron cyclotron maser," *Rev. Mod. Phys.*, Vol. 76, No. 2, 489–540, May 2004.
25. Barroso, J. J., R. A. Correa, and P. J. de Castro, "Gyrotron coaxial cylindrical resonators with corrugated inner conductor:

Theory and experiment," *IEEE Trans. Microwave Theory Tech.*, Vol. 46, No. 9, 1221–1230, Sep. 1998.

26. Iatrou, C. T., S. Kern, and A. B. Pavelyev, "Coaxial cavities with corrugated inner conductor for gyrotrons," *IEEE Trans. Microwave Theory Tech.*, Vol. 44, No. 1, 56–64, Jan. 1996.
27. Thumm, M., "State-of-the-art of high-power gyro-devices and free electron masers, Update 2008," Scientific Report FZKA 6224, Forschungszentrum Karlsruhe, Germany, Jan. 2008.
28. Singh, G., "Analytical study of the interaction structure of vane-loaded gyro-traveling wave tube amplifier," *Progress In Electromagnetics Research B*, Vol. 4, 41–66, 2008.
29. Qiu, C. R., Z. B. Ouyang, S. C. Zhang, H. B. Zhang, and J. B. Jin, "Self-consistent nonlinear investigation of an outer-slotted-coaxial waveguide gyrotron traveling-wave amplifier," *IEEE Trans. Plasma Sci.*, Vol. 33, No. 3, 1013–1018, Jun. 2005.
30. Kesari, V., *Analysis of Disc-loaded Circular Waveguides for Wideband Gyro-TWTs*, LAP-Lambert Academic Publishing AG & Co., Germany, 2009, ISBN: 978-3-8383-1145-6.
31. Kesari, V., P. K. Jain, and B. N. Basu, "Analytical approaches to a disc loaded cylindrical waveguide for potential application in wideband gyro-TWTs," *IEEE Trans. Plasma Sci.*, Vol. 32, No. 5, 2144–2151, Oct. 2004.
32. Kesari, V., P. K. Jain, and B. N. Basu, "Analysis of a circular waveguide loaded with thick annular metal discs for wideband gyro-TWTs," *IEEE Trans. Plasma Sci.*, Vol. 33, No. 4, 1358–1365, Aug. 2005.
33. Kesari, V., P. K. Jain, and B. N. Basu, "Analysis of a disc-loaded circular waveguide for interaction impedance of a gyrotron amplifier," *Int. J. Infrared and Millimeter Waves*, Vol. 26, No. 8, 1093–1110, Aug. 2005.
34. Kesari, V., P. K. Jain, and B. N. Basu, "Modeling of axially periodic circular waveguide with combined dielectric and metal loading," *J. Physics D: Applied Physics*, Vol. 38, 3523–3529, Sep. 2005.
35. Kesari, V., "Beam-absent analysis of disc-loaded-coaxial waveguide for its application in gyro-TWT (Part-1)," *Progress In Electromagnetics Research*, Vol. 109, 211–227, 2010.
36. Kesari, V., "Beam-present analysis of disc-loaded-coaxial waveguide for its application in gyro-TWT (Part-2)," *Progress In Electromagnetics Research*, Vol. 109, 229–243, 2010.
37. Choe, J. Y. and H. S. Uhm, "Theory of gyrotron amplifiers in

disc or helix loaded waveguides," *Int. J. Electron.*, Vol. 53, No. 6, 729–741, Jun. 1982.

38. Leou, K. C., T. Pi, D. B. Mcdermott, and Jr. N. C. Luhmann, "Circuit design for a wideband disc loaded gyro-TWT amplifier," *IEEE Trans. Plasma Sc.*, Vol. 26, No. 3, 488–495, Jun. 1998.
39. Yue, L., W. Wang, Y. Wei, and Y. Gong, "Approach to a coaxial arbitrary-shaped groove cylindrical waveguide for application in wideband gyro-TWTs," *IEEE Trans. Plasma Sc.*, Vol. 35, No. 3, 551–558, Jun. 2007.
40. Bratman, V. L., A. W. Gross, G. G. Denisov, W. He, A. D. R. Phelps, K. Ronald, S. V. Samsonov, C. G. Whyte, and A. R. Young, "High-gain wide-band gyrotron traveling wave amplifier with a helically corrugated waveguide," *Phys. Rev. Lett.*, Vol. 84, No. 12, 2746–2749, Mar. 2000.
41. Rao, S. J., P. K. Jain, and B. N. Basu, "Broadbanding of gyro-TWT by dielectric-loading through dispersion shaping" *IEEE Trans. Electron Dev.*, Vol. 43, No. 12, 2290–2299, Dec. 1996.
42. Rao, S. J., P. K. Jain, and B. N. Basu, "Hybrid-mode helix-loading effects on gyro-travelling-wave tubes," *Int. J. Electron.*, Vol. 82, No. 6, 663–675, Jun. 1997.